International Journal of Automotive Technology, Vol. 18, No. 3, pp. 377–385 (2017)
DOI 10.1007/s12239–017–0038–0

pISSN 1229–9138/ eISSN 1976–3832

NUMERICAL ANALYSIS AND EXPERIMENTAL STUDY ON THE PERFORMANCE OPTIMIZATION OF COLD STORAGE HEAT EXCHANGER INTEGRATED WITH EVAPORATOR

Daewoong Lee*

R&D Division, Halla-Visteon Climate Control Corp., 95 Sinilseo-ro, Daedeok-gu, Daejeon 34325, Korea

(Received 24 November 2015; Revised 13 May 2016; Accepted 5 September 2016)

ABSTRACT–The ISG (Idle Stop and Go) systems are commonly used in modern automobiles because they are economical and environmental friendly technology. However, when a vehicle stops, the air-conditioning system stops, resulting in thermal discomfort to passengers in the cabin. This paper examines a cold storage heat-exchanger (CSH) integrated with an evaporator. The position of the cold storage parts inside a heat exchanger was analyzed through numerical simulations using FLUENT to create an adequate design for a CSH. The CSH performance was then examined with various airflow volumes and optimized experimentally in terms of the refrigerant flow circuit and fin density in the heat exchanger. Next, an experiment on the coldness release performance of the CSH was conducted in the air-conditioning system. The cold storage system with optimized CSH experiment resulted in lower air discharge temperatures (3.5 °C ~ 4.9 °C) than current air-conditioning systems, and delayed the warm-up by approximately 155 seconds to reach 18 °C temperature of air discharge. For this study, the CSH is an effective solution for the ISG-applied vehicles with less investment by transforming current air-conditioners' structures more effectively.

KEY WORDS : Cold storage heat exchanger, Cold storage, Coldness release, Evaporator, Fuel economy, ISG, Latent heat, Numerical simulation, Phase change material, Thermal comfort

NOMENCLATURE

D	: depth (mm)
H	: height (mm)
L	: length (mm)
$\dot{m}$	: air flow volume rate (m^3/h)
P_{air}	: air pressure drop (Pa)
P_{ref}	: refrigerant pressure drop (kPa)
Q_c	: cooling capacity (kW)
t	: time (s)
T	: temperature (°C)
v	: velocity (m/s)

1. INTRODUCTION

The development trend of vehicles has increasingly been focusing on reducing fuel consumption and emissions. Until recently, the Idle Stop and Go (ISG) technology had only been applied to hybrid vehicles. Now, the ISG is being applied to internal combustion engine vehicles as well. According to several studies, the ISG automatically stops an engine when the engine is idling, such as waiting at traffic signals or temporary parking, to reduce exhaust emissions and improve fuel efficiency in stop-and-go traffic (Ao *et al*., 2007).

**Corresponding author.* e-mail: dlee6@hvccglobal.com

The current development trend in vehicle air-conditioning systems includes the realization of human-focused technology and improving thermal comfort. As an air-conditioner receives power from the compressor of the engine while driving, the ISG technology disturbs thermal comfort. Some tests have been conducted to improve the cabin comfort in two methods: first, by replacing the mechanical driving compressor with a motor-operated compressor run by electric energy; and second, by adding ice-storage devices to the air-conditioning system to supply cold air to the cabin when the engine stops to preserve comfortable temperatures (Guyonvarch *et al*., 2003).

Cold storage devices have been used for energy reduction for a long time in office buildings in the construction industry. Since it stores ice when the electric power load is low, such as at night in the summer, it provides cold air at the heat load peak time to reduce the need for electric power; thus, cold storage has received a great deal of attention as a green energy (Lee *et al*., 2013).

Numerical analysis of heat storage system using phase change material was conducted on vehicles (Lee *et al*., 1996). Yamada *et al*. (2013) conducted an experiment on the effects of cold storage on a climate-control wind tunnel by implementing a cold storage heat exchanger in the same shape as an evaporator which took twice as long to reach 15 °C. These tests were conducted in JC08 mode, which introduced a new chassis dynamometer test cycle for light

vehicles in Japanese 2005 emission regulations, on a vehicle to which the ISG technology was applied; the vehicle's mileage improved by less than 5 %.

Kowsky *et al*. (2014) developed an evaporator integral cold storage heat exchanger that applied thermo-siphon effects in order to respond to idle stops, and analyzed the freezing and melting points of phase change material filled in the heat exchanger. They conducted the study on a cold storage system that could minimize energy consumption through practical experiments.

Many efforts have been made to combine a cold storage heat exchanger and an evaporator in order to overcome the space limitation of a cabin in a vehicle where an air-conditioning system is located (Jeon *et al*., 2012; Jeon *et al*., 2013). Behr GMBH developed a heat exchanger that placed a cold storage on one side of an evaporator tube. When an air-conditioner works a cold storage tube is positioned adjacent to an evaporator tube through which refrigerant flows so ice can be stored in a minimal amount of time and then miniaturized (Cathy *et al*., 2002). Another cold storage heat exchanger integrated with an evaporator was also developed to replace a circular tube instead of a laminated plate-type heat exchanger (Hans, 2002).

Denso Co. designed that a cold storage heat exchanger positioned its refrigerant flowing passage in their evaporator, and cold storage materials entered its cold storage heat exchanger's passage dually in order to assign its cold storage function to its. The refrigerant flows inside the heat exchanger during cooling, while the cold storage materials fill the outer side storing ice (Yoshihiro *et al*., 2000; Kitamura *et al*., 2004).

Valeo Co. grafted a separate cold storage heat exchanger tube to the tube side of an evaporator to suggest how the two can be combined. The diameter of the hydraulic tube is larger than the existing tube through which refrigerant flows. This is made by a pressing method, and the tank in which the cold storage material is recharged is combined with the tank through which refrigerant flows (Regine *et al*., 2004).

Craig *et al*. (2010) conducted the study on the optimal driving strategy of a cold storage system considering fuel consumption and thermal comfort. They filled the phase change material in the upper part of an evaporator and used the thermal siphon effect, conveying this cold storage material to the evaporator's tube. They integrated the cold storage heat exchanger to repeat freezing and melting.

Lee *et al*. (2014) and Lee (2015) studied a cold storage evaporator consisting of an integral-type evaporator, and created a visualization of freezing and melting in the cold storage heat exchanger.

In this study, the cold storage heat exchanger combined with an evaporator was developed to provide thermal comfort of passengers, when air-conditioning systems turned off as the engine stops due to activation of ISG. When an air-conditioner was on, a cold storage heat exchanger used an evaporator and iced phase change material at the same time, and the air-conditioner was off, the latent heat released from the cold storage heat exchanger by melting phase change material in order to supply cold air to the cabin in a short time when the engine was stopped. The cold storage position in the heat exchanger was optimized by a numerical study.

When the cold storage heat exchanger created from the analysis was used as the air-conditioner, the refrigerant flow in the heat exchanger was examined in order to maintain the air-conditioning performance. As a result, the cooling capacity of the air side was optimized by changing the refrigerant flow path and fin density. Also, an optimized cold storage heat exchanger was installed in the air-conditioning system and when the compressor stopped, the discharge air temperature was compared to its current system's discharge air temperature.

2. EXPERIMENTAL APPARATUS AND METHOD

2.1. Numerical Analysis of Cold Storage Heat-exchanger

In the cold storage heat-exchanger (CSH), stacked laminated aluminum plates and louver fins, the coldness release performance of its cold storage piece is closely related to the volume of phase change material (PCM) and the location of it, as well as the evaporator performance. The selection of the optimal location was studied by the numerical simulations using a commercial CFD code (Hwang *et al*., 2010).

Governing equations of the simulation are the continuity equation, momentum equation, and energy equation. First, see the continuity equation as Equation (1).

$$\frac{\partial(\rho u_i)}{\partial x_i} = 0 \tag{1}$$

Momentum equation is as follows:

$$\frac{\partial(\rho u_i u_j)}{\partial x_j} = -\frac{\partial P}{\partial x_i} + \frac{\partial}{\partial x_j}\left[\mu\left(\frac{\partial u_i}{\partial x_j}+\frac{\partial u_j}{\partial x_i}\right) - \overline{\rho u_i' u_j'}\right] \tag{2}$$

where, $\overline{\rho u_i' u_j'}$ is Reynolds stress and is expressed according to Bossiness hypothesis, which is as follows:

$$\overline{\rho u_i' u_j'} = \mu_t\left[\frac{\partial u_i}{\partial x_j}+\frac{\partial u_j}{\partial x_i}\right] \tag{3}$$

Eddy viscosity μ_t is a function of turbulence momentum energy k and disappearance rate ε, as follows,

$$\mu_t = \rho C_\mu \frac{k^2}{\varepsilon} \tag{4}$$

Turbulence momentum energy k and disappearance rate ε are expressed by Equations (5) to (7).

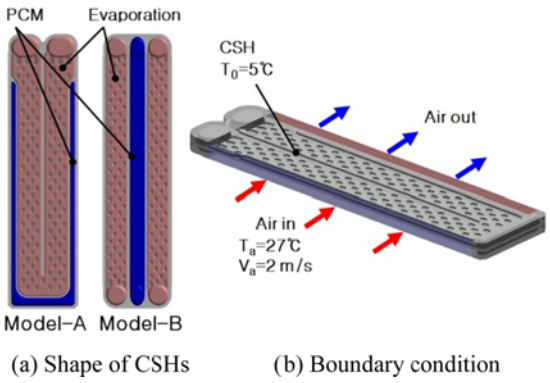

Figure 1. Numerical analysis model of CSHs.

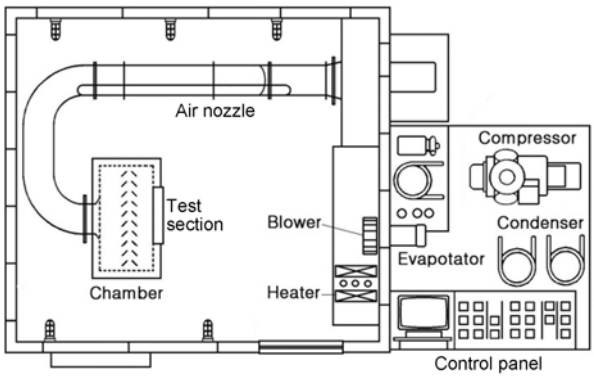

Figure 2. Schematic diagram of CSH calorimeter chamber.

$$\frac{\partial(\rho u_i k)}{\partial x_i} = \frac{\partial}{\partial x_i}\left(\frac{\mu_t}{\sigma_k}\frac{\partial k}{\partial x_i}\right) + G_k - \rho\varepsilon \tag{5}$$

$$\frac{\partial(\rho u_i \varepsilon)}{\partial x_i} = \frac{\partial}{\partial x_i}\left(\frac{\mu_t}{\sigma_\varepsilon}\frac{\partial \varepsilon}{\partial x_i}\right) + \frac{\varepsilon}{k}(C_{1\varepsilon}G_k - C_{2\varepsilon}\rho\varepsilon) \tag{6}$$

$$G_k = \mu_t\left(\frac{\partial u_i}{\partial x_i} + \frac{\partial u_i}{\partial x_j}\right)\frac{\partial u_i}{\partial x_i} \tag{7}$$

Simplified governing equation and turbulence equation are as follows in Equation (8).

$$\frac{\partial}{\partial x_k}(\rho U_k \phi) = \frac{\partial}{\partial x_k}\left(\Gamma_\phi \frac{\partial \phi}{\partial x_k}\right) + S_\phi \tag{8}$$

From Equation (8), the first term expressed a physical change in the control volume. The second term is a convection term. The left side of the second term is a diffusion term and the right side of the second term is the source term. The governing equation is changed as parameter ϕ, if $\phi = 1$ which is the continuity equation, ϕ has velocity, then momentum equation. Γ_ϕ and source term S_ϕ are expressed as the governing equation. In the same control volume, the difference equation is expressed by Equation (9) in the FVM (Finite Volume Method).

$$\phi_p \sum_i (A_i - S_p) = \sum_i (A_i \phi_i) + S_c \tag{9}$$

Simulation is conducted by using FLUENT with standard k-ε turbulence model and up-wind scheme for turbulence and momentum discretization method. Coupling method for pressure and velocity used SIMPLE algorithm (Yoon and Han, 2004).

The numerical simulation was carried out using the plates in Figure 1 of a CSH with symmetry boundary conditions since the same plates are consecutively laminated. Two types of models were analyzed. The cold storage part was positioned outside the heat exchanger plate in Model-A, whereas it was located in the center of the plates in Model-B.

The numerical domain was extracted from the CAD model. The number of the tetrahedral meshes for the CFD model is approximately 5 million cells. The flow of numerical domain is unsteady, three-dimensional, incompressible and turbulent. For the turbulence modeling, the standard k-ε turbulent model was used. The melting-solidification physical model was used to analyze the phase change of cold storage material. Figure 1 shows the numerical domain and its boundary conditions. Figure 1 (a) shows two types of CSHs. In Figure 1 (b), the boundary conditions of the upper and lower surfaces are symmetric.

To start the simulation, the temperatures of plates, PCM and refrigerant were initialized at 5 °C. The refrigerant was in a vapor state. As the air at 27 °C flowed through the domain, the CFD calculation was performed.

The result of the CFD from this study could be used to

Table 1. Specification of CSHs at calorimeter experiment.

No	Size (mm)	Ref. flow path	Fin density (FPDM)
Base	274W × 250H × 45D	7/20 → 12/15	68
#1	274W × 250H × 60D	7/20 → 12/15	54
#2	274W × 250H × 60D	7/20 → 16/11	54
#3	274W × 250H × 60D	7/20 → 19/8	54
#4	274W × 250H × 60D	7/20 → 19/8	62
#5	274W × 250H × 60D	7/20 → 19/8	68

Table 2. Experimental conditions of cooling performance at calorimeter.

Air inlet temperature	27 °C, 50 % RH
Air volume low rate	450 m^3/h
Refrigerant inlet pressure	1539.6 kPa
Refrigerant inlet temperature	54 °C
Refrigerant outlet pressure	5.5 °C

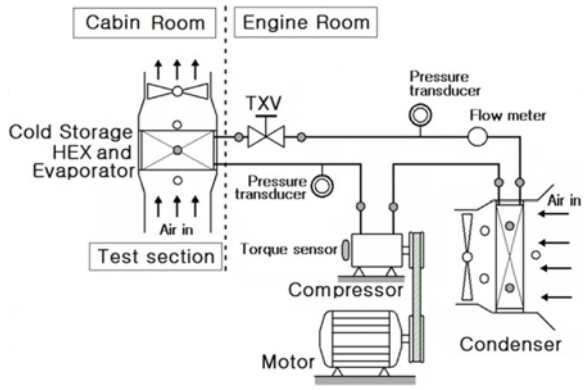

Figure 3. Schematic of cold storage system experiment apparatus.

predict the performance of a CSH.

2.2. Calorimeter of Cold Storage Heat-exchanger

Figure 2 shows a schematic diagram of the calorimeter used to test the performance of a CSH's evaporator. The guide vane is attached to the front side of a calorimeter to supply uniform airflow and thermally isolate to prevent any thermal loss which was compensated to make an accurate assessment. A closed-construction electric heater heated air evenly; it was chosen because its thermal density was lower than an open-type heater. An air-conditioner used for air cooling was controlled by a 22.4 kW compressor, an expansion valve, and an evaporation pressure controller. Also, two oil separators were installed in series for oil to maintain 3 % of refrigerant circulation to minimize any performance difference by the compressor oil.

The temperature was measured by an RTD sensor, including ± 0.01 °C sensing errors, at the inlet and outlet of the experiment part and the high and low air volumes were measured separately with the nozzle of a Brandt B-NZP1000, which is the measurement accuracy of air flow volume within ± 0.3 %. Humidity was supplied by steam at about 180 °C, heated by an electric heater, and its circulating refrigerant quantity was measured by the mass flow meter.

Table 1 displays the experimental results for the performance optimization of CSHs. The performance experiment was carried out at calorimeter with various heat exchangers that the refrigerant flow circuit and the fin density in the CSH for the same evaporation performance as a current evaporator (Base).

Table 2 shows the experimental conditions at a calorimeter chamber used for the evaporation performance experiment of CSHs.

2.3. Coldness Release Performance of Cold Storage Heat-exchanger

An experiment of a cold storage and coldness release was conducted in an air-conditioning system by optimizing a CSH at calorimeter.

Figure 3 shows the schematic diagram of the performance experiment apparatus of an air-conditioning system

Table 3. Air-conditioning system components with CSH.

Condenser	Type	PF type, 34 tubes
	Size	677W × 341H × 16D
Evaporator	Base	274W × 250H × 45D, 68FPDM
	CSH #4	274W × 250H × 60D, 62FPDM
	CSH #5	274W × 250H × 60D, 68FPDM
Compressor		VS18 Swash plate type
Thermal expansion valve		147 kPa at 0 °C, 250 kPa at 10 °C

Table 4. Experimental conditions of cold storage system performance of air-conditioner.

Cabin room	
Evaporator inlet temperature	24 °C, 35 % RH
Air volume flow rate	450 m^3/h
Engine room	
Condenser inlet air temperature	45 °C
Air volume flow rate	2745 m^3/h
Compressor rotational speed	2580 rpm

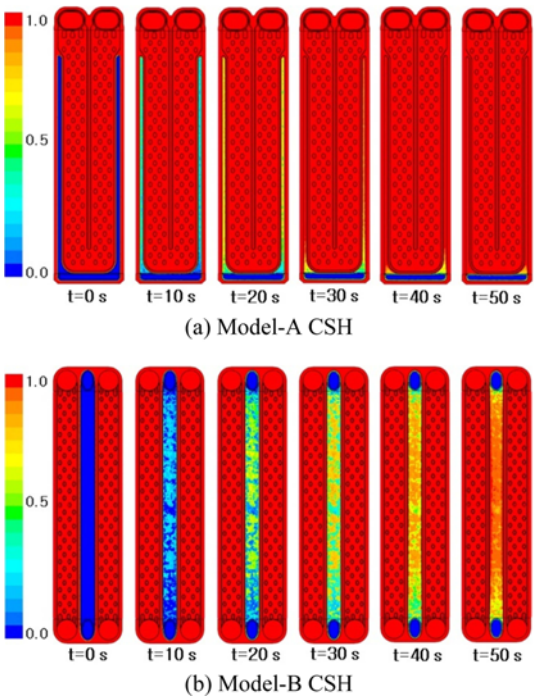

Figure 4. Numerical analysis results of liquid fraction of PCM.

equipped with a CSH. The actual vehicle's engine compartment and the inside were constructed for the performance experiment; each could be controlled independently in various environmental and operating conditions, such as temperature, humidity, airflow volume, and rotating speed of compressor.

The CSH's blown air temperature was controlled by the refrigerator installed in the test equipment and the electric heater. The airflow volume was controlled by separate nozzles. In addition, the rotating speed of its compressor, working torque, input power, refrigerant pressure, and temperature in the system were each measured and controlled, and the refrigerant mass flow rate in the system was measured by using the mass flow meter.

Table 3 details the specification of each component of an air-conditioning system used to experiment the cold storage and coldness release performance. The melting point of the PCM filled in the cold storage part was 6 °C, its freezing point was 2 °C, its heat of fusion was 214 kJ/kg, and its specific heat was 1.8 kJ/kg·K respectively.

The coldness release performance experiment of CSHs was conducted only for CSH #4 and CSH #5 in the same air-conditioning system. After that, the CSH was rated excellent in economic feasibility, evaporation performance, and applicability, compared to the current evaporator (Base) of an air-conditioner. Also, when the compressor stopped, the discharge air temperature and the effect of the CSHs were examined.

The detailed experimental condition is shown in Table 4. The airflow volume of 2745 m^3/h at 45 °C was set to the condenser, simulating the summer weather condition. During the test, the compressor rotated at 2580 rpm. At 24 °C, the temperature at which the interior became cold after running the air-conditioner in the summer, was set at the airflow volume of 450 m^3/h.

3. RESULTS AND DISCUSSION

3.1. Numerical Simulation Results of Cold Storage Heat-exchanger

It will be desirable to construct a CSH in an evaporator considering its effectiveness of ice storage, coldness release, and limited space. The numerical model was designed using Model-A and Model-B based on the patent survey and paper studies. Two CSHs were integrated with an evaporator, but the locations of the cold storage parts were different, as the volumes of the cold storage parts were the same size.

Figure 4 is the result of a numerical analysis of liquid fraction, and fusion-solidification for two CSHs model. The blue color, the solid (iced PCM) in the figure, is 0, and the red color, the liquid (melted PCM), is 1. The CSH in Model-A, its cold storage part is placed in both aspects of its heat exchanger. The PCM of the solid melted slowly and turned into liquid in 20 seconds. The CSH in Model-B, its cold storage part is placed in the center of its heat exchanger. The PCM of solid became liquid, but in 40 seconds.

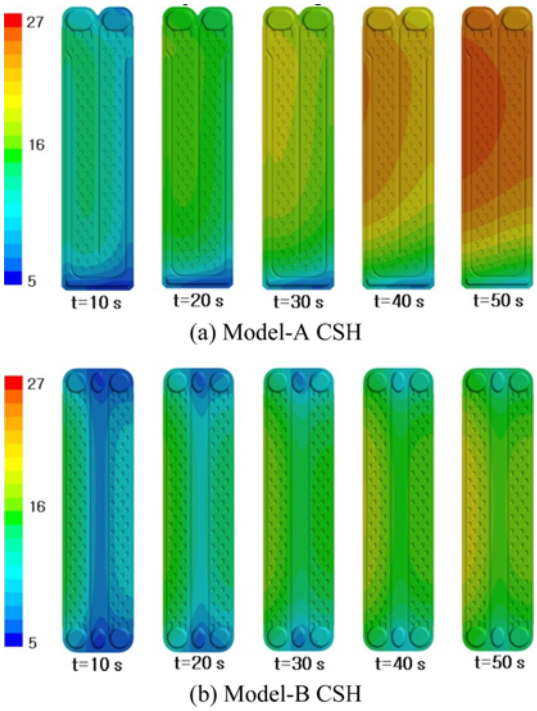

Figure 5. Numerical analysis results of surface temperature of CSHs.

The surface temperature changes of the two CSHs are compared in Figure 5. The blue color in the drawing is 5 °C, the temperature of the PCM and refrigerant was initialized at the start of the simulation, and the red color, which is the air temperature, is 27 °C. The surface temperature of the CSH in Model-A rapidly increased after 30 seconds, and most parts of the heat exchanger reached over 24 °C at 40 seconds.

Meanwhile, the surface temperature of the heat

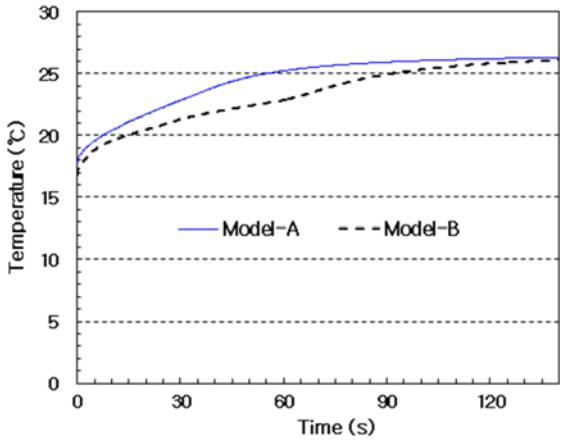

Figure 6. Numerical analysis results of discharge air temperature from CSHs.

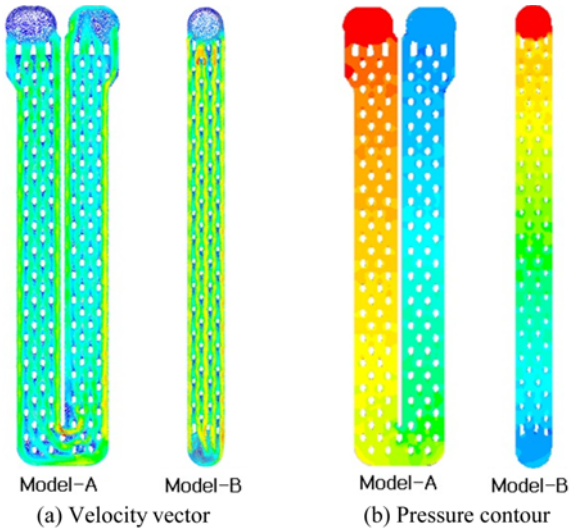

Figure 7. Numerical analysis results of refrigerant velocity and pressure contour for CSHs.

exchanger in Model-B did not rise sharply until 50 seconds. The cold storage portion located in both sides of the heat exchanger in Model-A, released coldness more quickly than on the cold storage portion located in the center of the heat exchanger in Model-B. As a result, liquefaction accelerated, and the surface temperature increased quickly in Model-A.

Figure 6 is the simulation results of discharge air temperature from the CSHs. The temperature of the discharge air in Model-B, cold storage portion to be located in the center of the heat exchanger was lower than Model-A.

Figure 7 shows the numerical analysis results of the refrigerant circuit for Model-A and Model-B. In Model-A, the refrigerant flows from the left tank to the right one. The U-turn flows cause a disturbance of refrigerant after the flow change. In Model-B, refrigerant flows from top to bottom, and has a relatively uniform flow circuit.

3.2. Performance Optimization of Cold Storage Heat-exchanger

Figure 8 compares the cooling capacities of various heat exchangers. A CSH integrated with an evaporator should maintain its evaporator performance of an air-conditioning system, which is the current evaporator function in addition to the cold storage portion. Therefore, to test the cooling capacity of a CSH, its internal refrigerant flow circuit was varied. Although the cooling capacity of CSH #3 was the best according to the experimental results at the airflow volume of 450 m^3/h, it was slightly inferior to the current evaporator performance (Base).

Figure 9 illustrates the detail results of the cooling capacity experiment from the CSH that was made by changing the refrigerant flow circuit in the heat exchanger depicted on Figure 8. CSH #3 evaluated cooling capacity,

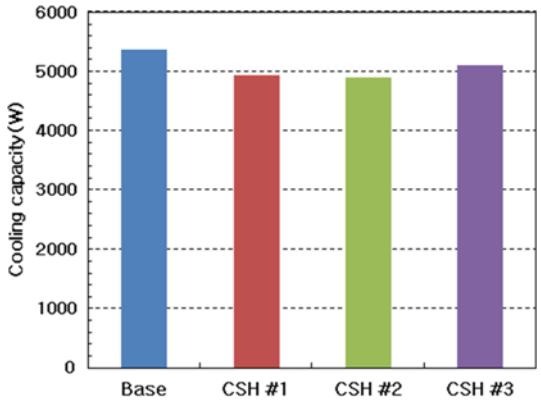

Figure 8. Comparison of cooling capacities with various CSHs (m = 450 m^3/h).

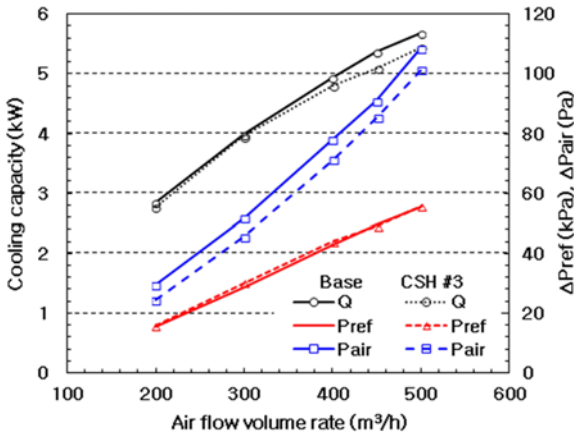

Figure 9. Comparison of cooling capacity, air pressure drop and refrigerant pressure drop with Base and CSH.

refrigerant pressure, and air pressure drop by changing the airflow volume.

Although the #3 was a slightly lower resistance in air pressure drop, the cooling capacity proved to be inferior from over 400 m^3/h of the airflow volume. According to this result, the CSH needs to improve its cooling capacity. For cooling capacity, uncertainty analysis was found to be .98 %. It was used as the uncertainty model proposed by Kline and McClintock (1953).

Figure 10 depicts the results of an experiment that measured cooling capacity, air pressure drop, and refrigerant pressure drop while changing an airflow volume for several fin densities by changing the pitch of other CSHs. In the air pressure drop shown on Figure 10 (a), the CSH #4 had a marginal increase at the airflow volume of 400 m^3/h compared to the Base. On the other hand, the air pressure drop of the CSH #5 was higher than the Base at the airflow volume of 200 m^3/h.

The cooling capacity was compared in Figure 10 (b). Both CSH #4 and CSH #5 excluding CSH #3, had the same cooling capacity as the Base, confirming that the cooling capacity has improved by controlling the fin density, and

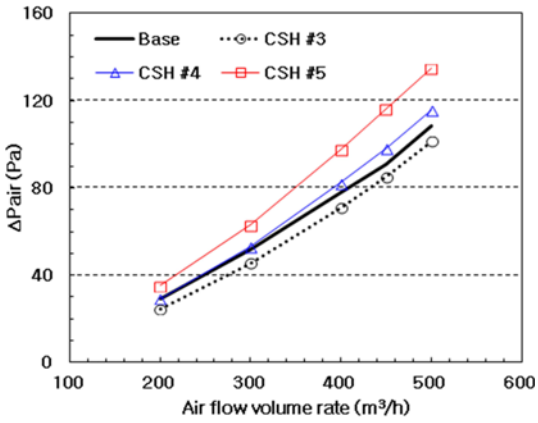

(a) Comparison of air side pressure drop

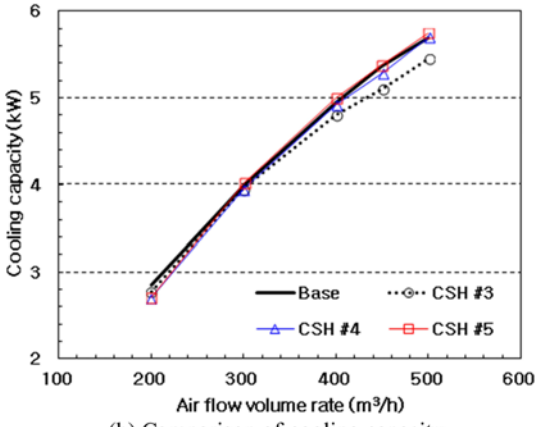

(b) Comparison of cooling capacity

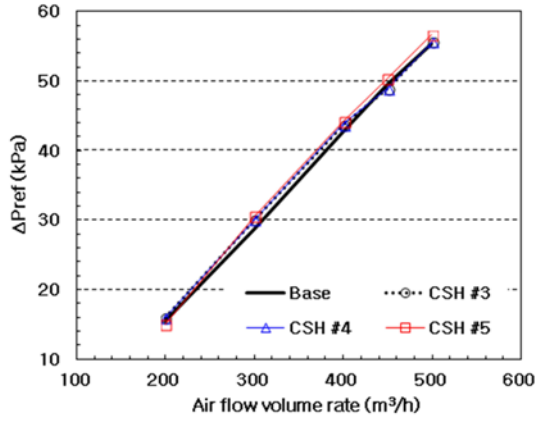

(c) Comparison of refrigerant side pressure drop

Figure 10. Experimental results of performance with Base and various CSHs.

uncertainties analyzed maximum 2.28 % among experimented heat exchangers.

Figure 10 (c) compared the refrigerant pressure drop and all the CSHs experimented, resulting in the same pressure drop as the Base.

3.3. Coldness Release Performance Results of Cold Storage Heat-exchanger

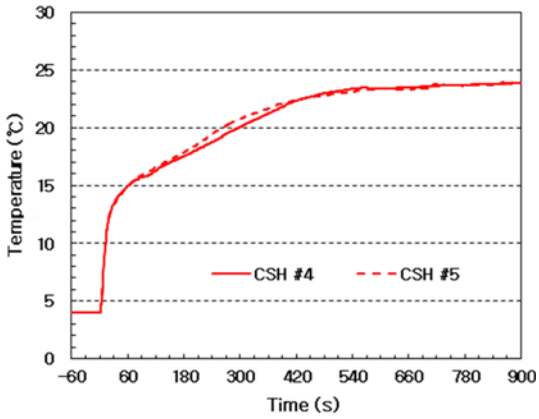

Figure 11. Experimental results of air discharge temperature with various CSHs.

A performance experiment for an air-conditioning system was carried out in order to confirm its coldness release performance of its CSH. Each air-conditioning component listed in Table 3 was installed to simulate an actual vehicle state accordingly, as well as for the CSH #4 and CSH #5, and the experimental conditions were stated in Table 4 for the air-conditioner. After enough cold storage was achieved, air was blown to the CSH, and the temperature of discharge air was changed as the PCM that melted down was examined.

Figure 11 measures the coldness release performance of CSH #4 and CSH #5. The temperature of discharged air rapidly increased after its compressor stopped. The results of temperature of air discharge for both CSH #4 and CSH #5 seemed similar; the air temperature of CSH #4 surpassed CSH #5's at 420 seconds. CSH #5 had a more rapid heat transfer because of its larger fin pitch. The coldness release performance was similar in both CSH #4, and CSH #5.

However, CSH #4 was ultimately selected as an excellent heat exchanger based on the experimental results.

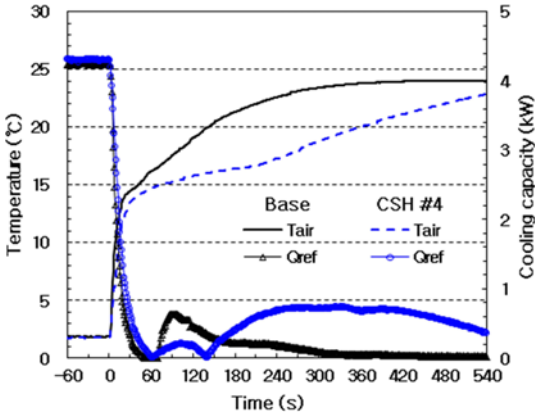

Figure 12. Comparison of coldness release performance with CSHs (m = 450 m^3/h).

Figure 12 compares the temperature of discharged air after the compressor stopped between the CSH and the current evaporator (Base).

The temperature of discharged air sharply increased after 60 seconds and exceeded 20 °C at 150 seconds. In the case of CSH #4, the increase temperature of discharged air was substantially delayed, and it reached 20 °C after about 6 minutes. There was a time delay in reaching the temperature of 18 °C for the CSH of about 155 seconds compared to the Base. Also, based on the traffic signal waiting or short parking time of 2 ~ 5 minutes, the temperature of discharged air was lower by approximately 3.5 °C ~ 4.9 °C compared to the Base.

With a compressor running, its cooling capacity of a current air-conditioner was around 4 kW. When it stopped, its cooling capacity dropped and its air temperature sharply increased after the refrigerant inside of the evaporator, heat-exchanger, vaporized. On the other hand, the CSH #4 secured its cooling capacity longer, as the PCM stored inside of the CSH melted down after the refrigerant in the evaporator vaporized.

4. CONCLUSION

This study examined the performance of an optimized CSH integrated with an evaporator in an effort to improve cabin thermal comfort when a compressor of an air-conditioning system stopped while an engine was in ISG mode. The following conclusions were found.

Model-B was selected by the results of the numerical analysis because its cold storage part was located in the center of a CSH.

The CSH was optimized experimentally when cooling capacity, air pressure drop, and refrigerant pressure dropped. As a result of the coldness release experiment of the CSH in the air-conditioning system, CSH #4 was rated excellent.

The discharged air temperature compared to the Base appeared to be 3.5 °C ~ 4.9 °C lower, and it was delayed by 155 seconds until it reached 18 °C in CSH #4.

The evaporator-integrated CSH developed from the results of this study has the same cooling capacity as the current evaporator and sufficient coldness release performance during short parking or the traffic signal waiting times due to the latent heat evaporation of PCM.

REFERENCES

Ao, G. Q., Qiang, J. X., Zhong, H., Yang, L. and Zhno, B. (2007). Exploring the fuel economy potential of ISG hybrid electric vehicles through dynamic programming. *Int. J. Automotive Technology* **8**, **6**, 781–790.

Cathy, B., Roland, B., Gottfried, D., Guenther, F., Kurt, M., Von, R. G., Wolfgang, S., Brigitte, T. R. and Marcus, W. (2002). Air-conditioning for Automobile. Patent No. JP2002-274165, Behr GMBH.

Craig, T., O'Brien, J., Polisoto, D. and Wolfe, N. (2010). Integrated air-conditioning evaporator with phase change material for thermal storage. *SAE Automotive Alternate Refrigerant Systems Symp.*, 10AARS-022.

Guyonvarch, G., Haller, R. and Lepetit, L. (2003). A comparison between climate control systems providing thermal comfort during vehicle stops. *SAE Paper No*. 2003-01-1073.

Hans, K. (2002). Heat Exchanger for Air Conditioner for Automobile. Patent No. JP2002-362138, Behr GMBH.

Hwang, J., Heo, H., Bae, S., Lee, D., Choi, H. and Kim, Y. (2010). Numerical evaluation of thermal flow characteristics of louvered fin type heat exchangers. *KSAE Annual Conf. Proc., Korean Society of Automotive Engineers*, 597–601.

Jeon, Y., Oh, K. and Wang, Y. (2012). Experimental study on cooling performance during ISG mode with cold storage evaporator. *KSAE Daejeon and Chungcheong Brench Conf*., 12-J0015, 19–25.

Jeon, Y., Oh, K., Jeong, S. and Wang, Y. (2013). Experimental study on cooling effect of cold storage system during ISG mode. *KSAE Annual Conf. Proc., Korean Society of Automotive Engineers*, 798–804.

Kitamura, K., Shirota, Y. and Takahashi, K. (2004). Vehicle Air-conditioner with Cold Accumulator. Patent No. US 6708512, Denso Corp.

Kline, J. J. and McClintock, F. A. (1953). Describing uncertainties in single-sample experiments. *Mechanical Engineering*, **75**, 3–9.

Kowsky, C., Wolfe, E., Chowdhury, S., Ghosh, D. and Wang, M. (2014). PCM evaporator with thermosiphon. *SAE Paper No*. 2014-01-0634.

Lee, D. (2015). Experimental study of the effect on cabin thermal comfort for cold storage systems in vehicles. *Trans. Korean Society of Automotive Engineers* **23**, **4**, 428–435.

Lee, D., Keon, D., Chung, S., Jeong, C. and Wang, Y. (2014). Performance investigation of cold storage heat-exchanger or vehicle applied ISG. *KSAE Annual Conf. Proc., Korean Society of Automotive Engineers*, 485–492.

Lee, K. H., Too, M. C. and Baek, N. C. (2013). Thermal storage control for zero-electric demand of low-energy solar house during on-peak period. *SAREK Winter Conf*., 13-W-075, 1067–1071.

Lee, K. S., Kim, H. J., Baek, C. I., Song, Y. K., Han, C. S. and Kim, D. J. (1996). Numerical analysis on the performance for automobile heat storage system using phase change material. *Trans. Korean Society of Automotive Engineers* **4**, **3**, 187–198.

Regine, H., Didier, L., Loic, L. and Christian, P. (2004). Thermal-inertia Heat Exchanger for Automobile Cooling Liquid Circuit. Patent No. JP2004-184071, Valeo Climatisation.

Yamada, A., Nishida, S., Yokoyama, N., Abei, J., Danjo, T., Florida, L., Brodie, B. and Nagano, Y. (2013). Cold

storage air conditioning system for idle stop vehicle. *SAE Paper No*. 2013-01-1287.

Yoon, C. S. and Han, S. (2004). CFD analysis for the flow phenomena of the narrow channels in plate heat exchanger for intercooler. *Trans. Korean Society of Automotive Engineers* **12**, **2**, 91–100.

Yoshihiro, I., Yashhiko, N. and Shin, N. (2000). Heat Storage Heat Exchanger Apparatus and Vehicle Air Conditioning Apparatus. Patent No. JP2000-205777, Denso Corp.